Available online at www.sciencedirect.com
ScienceDirect
Journal of Power Sources 167 (2007) 18–24
JOURNAL OF POWER SOURCES
www.elsevier.com/locate/jpowsour

Electrochemical synthesis of Fe–Mo and Fe–Mo–Pt alloys and their electrocatalytic activity for methanol oxidation

F. Shafia Hoor, C.N. Tharamani *, M.F. Ahmed, S.M. Mayanna **

Department of Post-Graduate studies and Research in Chemistry, Central College, Bangalore University, Bangalore 560001, India

Received 12 December 2006; received in revised form 1 January 2007; accepted 2 January 2007
Available online 12 February 2007

Abstract

Electroplating of Fe–Mo and Fe–Mo–Pt alloys has been carried out using suitable plating bath solutions and working conditions. The deposits were characterized by SEM, XRD, TEM, EDAX, XPS and Polarization techniques. New phases appeared on heat treatment of the coatings. The composition (Fe–Mo) of the coatings and oxidation states of the alloying elements varied from the surface to the bulk of the material. The coatings acted as novel electrode materials with good electrocatalytic activities (low overpotentials) and good corrosion resistance for the anodic oxidation of methanol in H_2SO_4 at normal working temperature. The good corrosion resistance of the Fe–Mo alloy is accounted for by the existence of an oxyhydroxide passive film on the surface. The electrocatalytic activity of the Fe–Mo–Pt alloy is considerably higher when compared to the Fe–Mo alloy and Fe alone

Keywords: Alloys; Anode; Electrocatalytic activity; Fuel cell; Corrosion resistance

1. Introduction

In view of the rapid growth of world population and the depletion of non renewable fossil fuel, the search for new non-conventional renewable electrical energy has become a subject of importance in recent years. Among many non-conventional alternative electrical energy sources, electrochemical energy conversion through the use of fuel cell has gained importance. Fuel cells convert the chemical energy of a fuel directly into electricity and since fuel cells operate without a thermal cycle, they constitute one of the most promising sources of alternative electrical energy, by providing high-energy output and in theory emitting no harmful by-products. Fuel cells also require no emission-control devices as in conventional energy-conversion [1–3]. There are six types of generic fuel cells among these, direct methanol fuel cells are promising systems for portable and residential power applications [4].

Although a lot of progress has been made in the development of the direct methanol fuel cell (DMFC), its performance is still limited by the poor kinetics of the anode reaction [5–7] and the crossover of methanol from the anode to the cathode side through the proton exchange membrane [8–10]. Electrocatalysts with a higher activity for methanol oxidation at room temperature are critically needed to enhance DMFCs' performance for commercial applications. Although platinum shows excellent initial catalytic activity in the electrochemical oxidation of methanol at low temperatures, it is readily poisoned by chemisorbed CO-like intermediates generated in the process. Many researchers indicate that the alloying of Pt with the other transition metals enhances significantly the electrocatalytic activities and poison tolerance of Pt on the basis of a bifunctional mechanism, an electronic effect, or an ensemble effect [11–13]. Currently, a well known anode catalyst for DMFC is PtRu, because it gives significant activity for methanol oxidation as well as dehydrogenation of water which is critical for the removal of the adsorbed CO species [14–18] but still is not good enough for commercial applications due to its prohibitively high cost and limited supply. As a result, the development and characterization of a better poison-tolerant catalyst is of tremendous interest to this technology [19–22]. By eliminating Pt completely or using it in traces in the electrodes it is possible to reduce the cost of making a fuel

* Corresponding author. Present address: Department of Chemistry, University of Saskatchewan, #165-110 Science Place, Saskatoon SK S7N59, Canada. Tel.: +1 306 966 1453; fax: +1 306 966 4730.
** Corresponding author. Tel.: +91 80 23301726.
E-mail addresses: thara9@gmail.com (C.N. Tharamani), smm_chem@yahoo.com (S.M. Mayanna).

0378-7753/$ – see front matter © 2007 Elsevier B.V. All rights reserved.
doi:10.1016/j.jpowsour.2007.01.089

cell by 20% [23]. In this direction, attempts have been made to prepare and characterize novel material with low over potential and low priced alloys as anode materials for methanol oxidation fuel cell in H_2SO_4 could be based on the use of the use of two complementary characteristics of electrodeposits namely, intrinsic catalytic activity and high surface area [24–26].

Mo is a versatile metal and its alloys with iron group metals are used as effective cathode materials for water electrolysis [27,28]. These alloys are obtained from mechanosynthesis [29], thermal preparation [30] and electrodeposition [31] of which electrodeposition provides alloys with a wider range of compositions. The surface activity of these alloys depends on the pH of the working medium, composition, nature of the surface (crystalline/amorphous) and the phases present in the alloy [32,33]. The present communication reports the results of electrochemical preparation and characterization of Fe–Mo and Fe–Mo–Pt alloys as an anode for methanol oxidation in H_2SO_4 media. The anode materials developed are cost effective, the method of preparation is simple and offers a low overpotential for the oxidation reaction under normal working conditions. The influence of the surface features and structure of the alloy, and the post treatment of the alloy on electrocatalytic activity is discussed.

2. Experimental

All solutions were prepared by using AR Grade chemicals and double distilled water. Alloys of Fe–Mo and Fe–Mo–Pt were coated on copper foils (99% pure, 10 mm × 10 mm × 0.25 mm) using a suitable bath solution. Prior to deposition, copper foils were pre-cleaned by the procedures described elsewhere [34]. Polarization on prepared alloy samples were carried out in $CH_3OH + H_2SO_4$ mixture under galvanostatic condition using a potentiostat/galvanostat (EG & G PAR 362). A large platinum foil and saturated calomel electrode were used as auxiliary and reference electrodes, respectively. A fine-drawn capillary was used to minimize IR drop.

X-ray diffraction (XRD) patterns of deposited films were obtained on a Philips, PW 1140/90 diffractometer using Cu K_α radiation and Ni filter. Transmission electron microscopic (TEM) investigation of the film was carried out in a JEOL 200-CX transmission electron microscope operated at 200 kV. The elemental analyses and surface composition of the alloy samples were obtained by energy dispersive X-ray analysis (EDAX). Few alloy samples were given heat treatment (623 K) for 5 h under N_2 atmosphere.

X-ray photoelectron spectra (XPS) of the deposited alloys were recorded on a vacuum generator ESCA-III Mark 2 spectrometer (VG Scientific Ltd., England) using Al K_α radiation with photon energy of 1486.6 eV. The binding energies were calculated with respect to C (1s) peak at 285 eV with a precision of ± 0.2 eV. For XPS analysis, the samples were placed into an ultra high vacuum (UHV) chamber at 10^{-9} Torr housing the analyzer. Prior to mounting, the samples were kept in the preparation chamber at ultra high vacuum for 5 h in order to desorb any volatile species present on the surface. Intermittent sputtering was performed by using defocused Ar^+ ion beam at low voltage and current over an area of $0.8 \times 2.4\ mm^2$.

Sputtering was carried out to remove successive layer of few angstroms and composition of the material in the particular layer. The experimental data were curve fitted with Gaussian peaks after subtracting a linear background. For Gaussian peaks, slightly different full width at half maximum (FWHM) was used for different chemical states. The spin orbit splitting and the doublet intensities were fixed as given in the literature [35]. The concentrations of different chemical states were evaluated from the area of the respective Gaussian peaks.

3. Results and discussion

Experiments were carried out under potentiostatic conditions (−1000 to −1800 mV) in a bath solution containing known concentrations of ferrous ammonium sulphate, ammonium molybdate, TAC, chloroplatinic acid and EDA. Boric acid and sodium chloride were used as buffering agent and conducting electrolyte, respectively, and also the combination of them suppress to reduce the rate of codeposition of H_2 gas [36]. Experiments were conducted at different deposition potentials, bath compositions, pH and working temperature. Based on the experimental observations, the bath composition and working conditions were optimized (Table 1) to get good quality Fe–Mo and Fe–Mo–Pt alloys. The alloy coatings obtained under different experimental conditions were subjected to surface, microstructural and electrocatalytic analysis.

3.1. Microstructure and surface characterisation

The coatings obtained under optimum experimental conditions were subjected to EDAX analysis in order to determine the chemical composition of the coatings and to investigate the distribution of the elements on the electrode surface, which confirmed the presence of Fe(78%), Mo(22%) and Pt [in traces(<1%)] on the deposited surface (Fig. 1). In order to

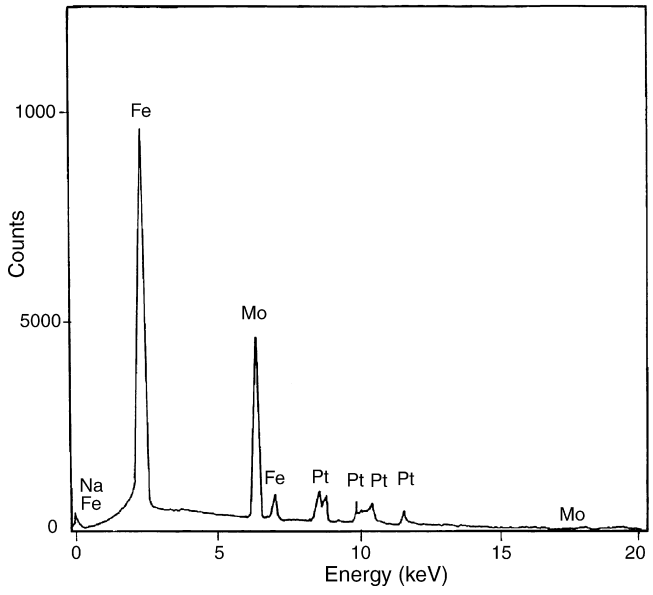

Fig. 1. Energy dispersive X-ray analysis of Fe–Mo–Pt alloy (as deposited).

Table 1
Bath composition and plating conditions for Fe–Mo, Fe–Mo–Pt alloy coating

Bath composition (M)	Fe–Mo (95–5%)	Fe–Mo (78–22%)	Fe–Mo–Pt (78-22%-traces)
Ferrous Ammonium Sulphate	0.14	0.10	0.10
Ammonium Molybdate	0.015	0.08	0.08
Tri ammonium Citrate	0.10	0.30	0.30
Ethylenediammine	0.10	0.03	0.03
Chloroplatinic acid[a]	–	–	10
Sodium chloride[b]	10	10	10
Boric acid[b]	20	20	20
Deposition potential (mV)	−1400	−1400	−1400
Time	1–2 h	1–2 h	1–2 h
pH	9.0	9.0	9.0
Cathode	Copper foil		
Temperature	303 K		
Anode	Stainless steel		

The composition of the element from EDAX analysis are values given in parenthesis.
[a] mM.
[b] g L^{-1}.

examine the morphology of the electroactive coatings used in research, a scanning electron microscopy (SEM) technique was used. The SEM images in Fig. 2 show significant differences in morphology of the investigated catalytic coatings. As deposited Fe–Mo alloy coating (Fig. 2A) shows a relatively homogeneous surface of small roughness. The morphology of the surface is in accordance with the crystalline structure obtained by the XRD analysis and the micrograph taken at a higher magnification showed polygonal forms characteristics of a crystalline structure. On the other hand, it can be observed that after heat-treatment of Fe–Mo (Fig. 2B) and incorporation of Pt (Fig. 2C) in traces show a spherical (globular) and cauliflower-like pattern, having a considerably rougher surface than as deposited Fe–Mo alloy and roughness increases in presence of Pt. This suggests an increased activity towards DMFC. It can also be observed on both (Fig. 2B and 2C) that some smaller ellipsoid-shaped globules appear on top of the larger globules. The borders of both smaller and bigger globules are circular or quasi-circular, which is quite different than the as deposited Fe–Mo alloy. The EDAX dot mapping of Pt and Mo are shown in Fig. 2D and 2E, respectively.

The XRD data (Table 2) of the Fe–Mo alloy (JCPDS: 15–0539) indicates the crystalline nature and also the presence of oxide in the alloy. Heat-treated samples show the existence of new phases (JCPDS: 22–0629) along with the presence of oxide phases H_2MoO_5 (JCPDS: 41–0359). XRD patterns (graphs are not shown here) of the deposited Fe–Mo–Pt alloy also showed similar trend along with small intense peak (trace amount of Pt) of platinum oxide (JCPDS: 85–0714) leads to the change in structure of the electrode surface, which is in accordance with the SEM micrographs. The ring type diffraction pattern of the Fe–Mo coating is shown in Fig. 3A, which could be indexed as Fe–Mo alloy supporting the XRD results [37]. The selected area electron diffraction (SAED) pattern is shown in Fig. 3B show crystalline nature of the Fe–Mo alloy.

3.2. X-ray photoelectron spectroscopic studies

XPS of Fe(2p) core level regions of as deposited Fe–Mo alloy sample as well as the same after 10 and 20 min of sputtering are shown in Fig. 4. It is observed that Fe is in +3 oxidation state along with satellite peaks. Fe($2p_{3/2,1/2}$) peaks at 711.5 and

Table 2
XRD data of Fe–Mo and Fe–Mo–Pt alloys

	As deposited			After heat treatment[a]		
	Observed 2θ	Std. ASTM[b] 2θ	Phase	Observed 2θ	Std. ASTM[b] 2θ	Phase
Fe–Mo Alloy	36.51	36.506	FeMo(311)	15.68	15.67	H_2MoO_5(101)
	41.72	41.72	FeMo(330)	30.89	30.88	$FeMoO_4$(111)
	44.83	44.83	FeMo(411)	36.51	36.506	FeMo(311)
				41.72	41.72	FeMo(330)
				44.83	44.83	FeMo(411)
Fe–Mo–Pt Alloy	36.51	36.506	FeMo(311)	15.68	15.67	H_2MoO_5(101)
	41.72	41.72	FeMo(330)	30.89	30.88	$FeMoO_4$(111)
	44.83	44.83	FeMo(411)	36.51	36.506	FeMo(311)
	46.24	46.24	Pt(200)	41.72	41.72	FeMo(330)
	44.83	44.83	FeMo(411)	41.98	41.99	PtO(110)

Target: Cu k_α; filter: Ni.
[a] 623 K under N_2 atmosphere for 5 h.
[b] 1999 JCPDS-International Centre for Diffraction Data, PCPDFWIN v. 1.30.

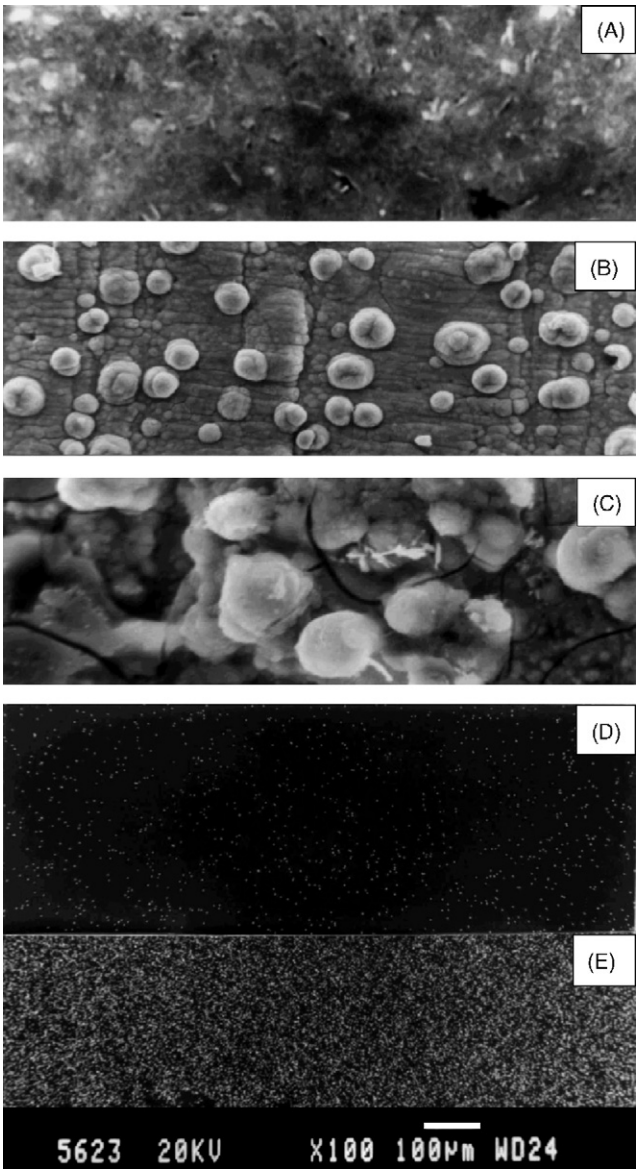

Fig. 2. SEM microphotographs of (A) as deposited Fe–Mo (22% Mo) alloy (B) heattreated Fe–Mo alloy (C) heat treated Fe–Mo–Pt alloy (D) dot mapping of Pt and (E) dot mapping of Mo element.

725.6 eV are attributed to Fe^{3+} oxidation state [38]. Similarly with the sputtered film of Fe($2p_{3/2,1/2}$) peaks are observed at 704.4 and 720.5 eV which are characteristic to Fe^0 state, respectively, with satellite peaks. Binding energies of Fe^{3+} and Fe^0 species of as deposited Fe–Mo film are given in Table 3.

The XPS spectra of Mo(3d) exhibits the characteristic $3d_{5/2}$ and $3d_{1/2}$ doublet (Fig. 5), associated with spin-orbit coupling for Mo. As deposited film shows Mo($3d_{5/2,3/2}$) broad peaks at 232.2 and 235.8 eV corresponding to Mo^{6+} oxidation state. After sputtering for 10 and 20 min, Mo($3d_{5/2}$) sharp peak appeared at 227.8 due to metallic Mo whereas Mo($3d_{3/2}$) broad peak appeared at 235.4 eV corresponding to Mo^{6+} [39].

Fig. 6 represents the XPS spectrum of oxygen 1s level for the deposited samples and after sputtering. O(1s) spectrum in deposited film shows intense peak at 531.7 eV together with a weak peak at 530.0 eV. The lower binding energy peak at

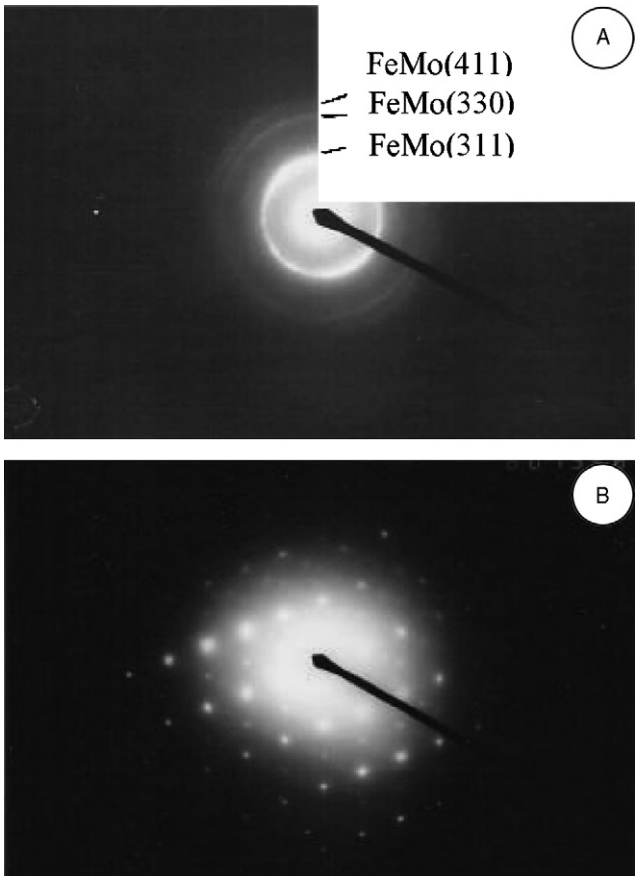

Fig. 3. (A) Ring type electron diffraction pattern; (B) selected area electron diffraction pattern (SAED) of as deposited Fe–Mo alloy.

530.0 eV is due to O^{2-} species associated with oxides of nickel and iron. The highly intense peak at 531.7 could be due to OH^- type of species and a weak peak at 533.7 eV indicates the presence of H_2O, which decreases on sputtering. The binding energies of O(1s) peaks in deposited sample and after sputtering are given in Table 3.

Although there is uncertainty in the assignment of the surface species from the XPS data, Mo^{6+} seems to be the most probable surface species, which forms the basis for the formation of the

Table 3
Binding energies of Fe($2p_{3/2}$), Mo($2p_{3/2}$) and O(1s) species of deposit and sputtered Fe–Mo alloy

Chemical state	Binding energy (eV)
Fe($2p_{3/2}$)	
Fe^{3+}	711.5
[a]Fe^0	704.4
Mo($3d_{5/2}$)	
Mo^{6+}	232.2
Mo^0	227.8
O(1s)	
O^{2-}	530.0 (530.2)
OH^-	531.7 (532.0)
H_2O	533.7 (533.5)

[a] Values for O^{2-}, OH^- and H_2O species after 10 min sputtering.

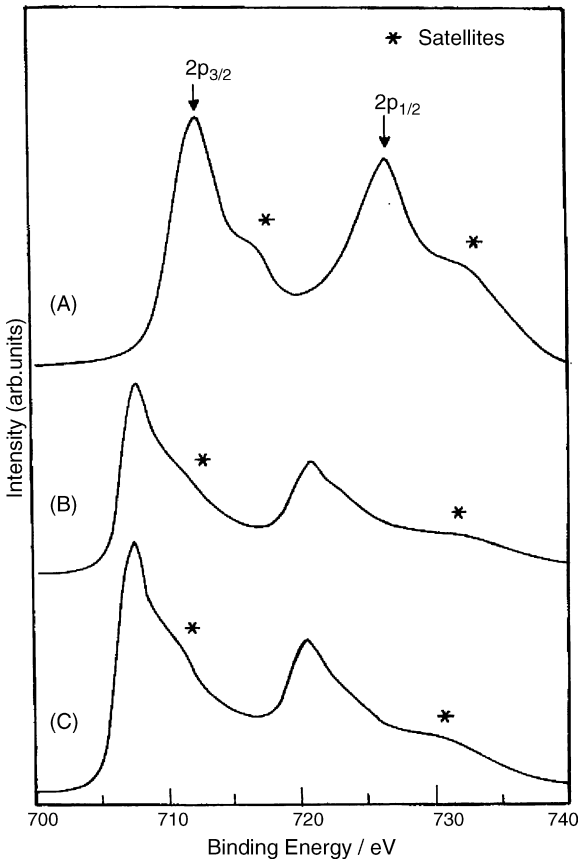

Fig. 4. XPS of Fe(2p) core level region of Fe–Mo alloy (A) as deposited (B) after 10 min sputtering (C) after 20 min sputtering.

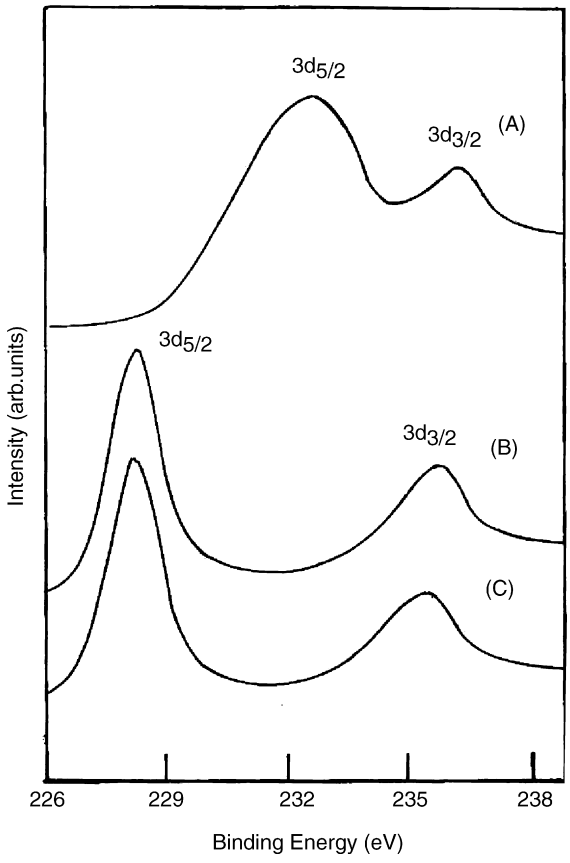

Fig. 5. XPS of Mo(3d) core level regions of Fe–Mo alloy (A) as deposited (B) after 10 min sputtering (C) after 20 min sputtering.

hydrous molybdenum oxide (H_xMoO_5) [40]. XRD studies also revealed that there is formation of oxide in the alloy, the extent of which increased on heat treatment. It is reported earlier that the sample under goes transition from hydroxides to oxides after heat treatment. The change in chemical state of Fe–Mo from hydroxide to oxide occurs with loss of oxygen and hydrogen (in the form of water molecules). These results show that the film is a mixed oxyhydroxides of Fe–Mo, which upon passivation improves the corrosion resistance of Fe–Mo alloy. Binding energies of different Mo species of as deposited Fe–Mo film are given in Table 3.

The concentration ratio of Fe(2p) to Mo(3d) on the surface can be evaluated using the relation:

$$\frac{C_{Fe}}{C_{Mo}} = \frac{I_{Fe}\sigma_{Mo}\lambda_{Mo}D_E(Mo)}{I_{Mo}\sigma_{Fe}\lambda_{Fe}D_E(Fe)}$$

Where, C, I, σ, λ and D_E are the concentration, intensity, photoionization cross-section, mean escape depth and geometric factor, respectively. Integrated intensities of Fe(2p) and Mo(3d) peaks are taken into account for calculating the concentrations. Photoionization cross-sections and mean escape depths are obtained from the literature [41,42]. The surface concentration ratio of Fe to Mo is 6.0 in the deposited film indicating surface enrichment of Fe. However, this ratio decreased on successive sputtering and it was found to be 1.5 and 0.3 after 10 and 20 min of sputtering, respectively.

3.3. Polarization studies

In order to test the suitability of the deposited Fe–Mo and Fe–Mo–Pt alloys for anodic oxidation of methanol, galvanostatic polarization experiments were conducted with coatings of different compositions (Mo 5–25%) during oxidation of methanol (1 M) in 0.5 M H_2SO_4 in a current density range

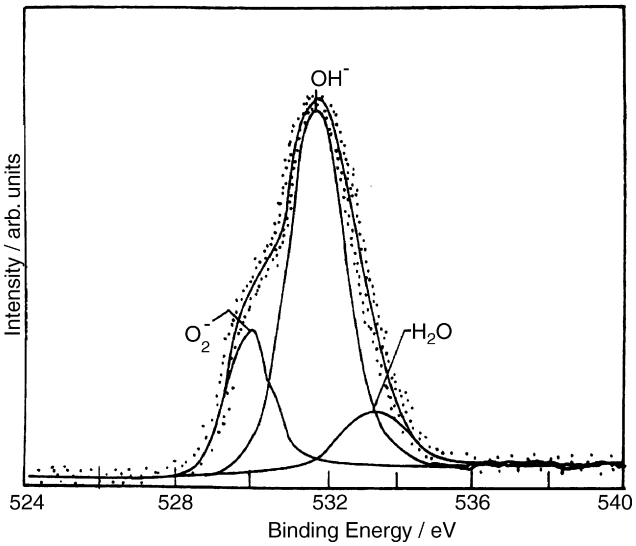

Fig. 6. XPS of O(1s) core level regions of Fe–Mo alloy.

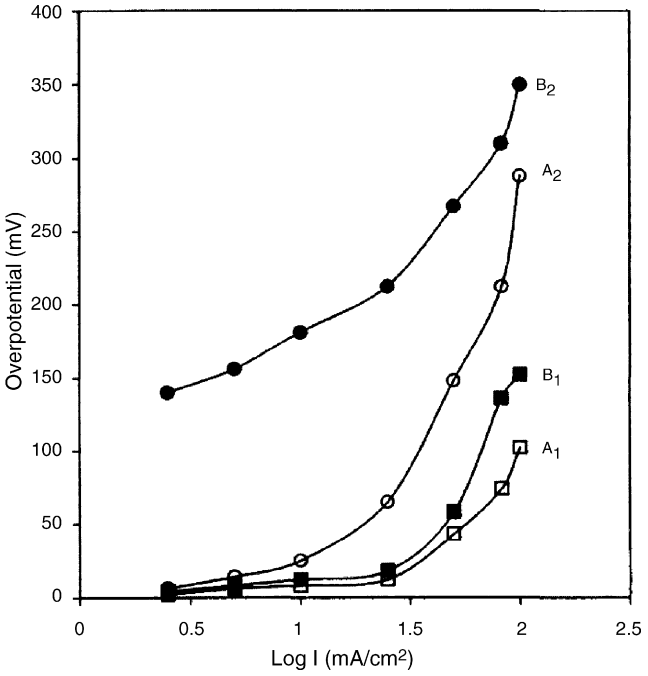

Fig. 7. Galvanostatic polarization diagrams for methanol oxidation in 0.5 M H_2SO_4, on (A) Fe–Mo–Pt and (B) Fe–Mo alloys of as deposited [A_2 and B_2] and after heat treatment [A_1 and B_1].

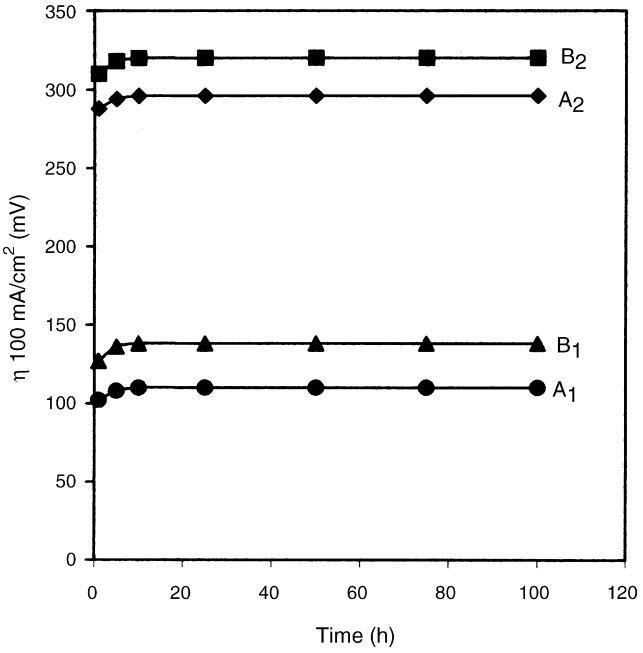

Fig. 8. Variation of over potential (η at 100 mA cm^{-2}) 1M CH_3OH + 0.5M H_2SO_4 with time on (A) Fe–Mo–Pt and (B) Fe–Mo alloys of as deposited [A_2 and B_2] and after heat treatment [A_1 and B_1].

1–100 mA cm^{-2} at 303 K. The electrocatalytic activity (η_{100}) was minimum for 5% Mo in the alloy and the activity increased with increase in the Mo content in the alloy and was maximum for 22% of Mo in the alloy. Pt was introduced in trace amount (<1%) in to the alloy with Mo −22% and the activity was found to increase sharply. Fig. 7 shows the galvanostatic anodic polarization of the as deposited and heat treated Fe–Mo (22% Mo) and Fe–Mo–Pt (78-22-traces) coatings in H_2SO_4 medium. The electrochemical parameters are given in Table 4. The overpotentials observed for methanol-oxidation on Fe–Mo–Pt coatings in H_2SO_4 was relatively less than that for Fe–Mo coatings as the working electrode. This suggests that traces of Pt in a dispersed state with Fe–Mo serves as a better electrocatalyst for the methanol oxidation than Fe–Mo.

The Fe–Mo and Fe–Mo–Pt alloys show better corrosion resistance (Table 4) in H_2SO_4. The heat treatment resulted in further improvement in the corrosion resistance. This was evident from the prolonged electrolysis (up to 100 h) conducted in 0.5 M H_2SO_4 containing 1M methanol at 303 K and a current density of 100 mA cm^{-2}. The anode was stable and exhibited steady overpotential (±10 mV) (Fig. 8), which is a key desirable characteristics of a high performing anode in a fuel cell.

Table 4
Electrochemical parameters for methanol oxidation in 0.5 M H_2SO_4 and 1 M CH_3OH on Fe–Mo (95–5%), Fe–Mo (78–22%), Fe–Mo–Pt (78–22-traces) alloys at 303 K

System	b_a (mV dec^{-2})	i_{corr} (μA cm^{-2})	η_{100} (mV)
Fe–Mo (95-5)	48 (58)	62 (35)	415 (310)
Fe–Mo (78-22)	32 (34)	55 (20)	350 (288)
Fe–Mo–Pt (78-22-traces)	48 (52)	10 (1.25)	152 (102)

The values for heat treated (5 h, N_2 atmosphere at 623 K) samples are given in the parenthesis.

4. Conclusions

Simple bath solutions and plating conditions were developed to deposit Fe–Mo and Fe–Mo–Pt alloys as anodes for direct methanol fuel cells. The deposited Fe–Mo alloy is crystalline in nature and new phases appeared on heat treatment. The composition of the alloying elements and their oxidation states varied from the surface to the bulk of the deposits. The alloys on heat treatment exhibited good corrosion resistance towards the fuel cell electrolytes.

Acknowledgements

One of the authors (F. Shafia Hoor) wishes to thank CSIR, New Delhi for providing the financial assistance in the form of Senior Fellowship to carryout this work.

References

[1] J. Larminie, A. Dicks, Fuel Cell Systems Explained, Wiley, New York, 2000.
[2] K. Kordesch, G. Simader, Fuel Cells and Their Applications, VCH, Weinheim, 1994.
[3] A. Hamnett, Philos. Trans. R. Soc. London A 354/1653 (1996).
[4] A.S. Aricò, S. Srinivasan, V. Antonucci, Fuel Cells 1 (2001) 1.
[5] E. Reddington, A. Sapienza, B. Gurau, R. Viswanathan, S. Sarangapani, E.S. Smotkin, T.E. Mallouk, Science 280 (1998) 1735.
[6] T. Iwasita, F.C. Nart, J. Electroanal. Chem. 317 (1991) 291.
[7] T.D. Jarvi, S. Sriramulu, E.M. Stuve, J. Phys. Chem. B 101 (1997) 3646.
[8] A. Heinzel, V.M. Barragan, J. Power Sources 84 (1999) 70.
[9] J. Cruickshank, K. Scott, J. Power Sources 70 (1998) 40.

[10] K. Ramya, K.S. Dhathathreyan, J. Electroanal. Chem. 542 (2003) 109.
[11] K.W. Park, J.H. Choi, B.K. Kwon, S.A. Lee, Y.E. Sung, H.Y. Ha, S.A. Hong, H. Kim, A. Wieckowski, J. Phys. Chem. B 106 (2002) 1869.
[12] S.A. Lee, K.W. Park, J.H. Choi, B.K. Kwon, Y.E. Sung, J. Electrochem. Soc. 149 (2002) 1299.
[13] K.W. Park, K.S. Ahn, J.H. Choi, Y.C. Nah, Y.M. Kim, Y.E. Sung, Appl. Phys. Lett. 81 (2002) 907.
[14] X. Zhang, Y.K. Chan, Chem. Mater. 15 (2003) 451.
[15] C. Lu, C. Rice, R.I. Masel, P.K. Babu, P. Waszczuk, H.S. Kim, E. Oldfoe, A. Wieclpwski, J. Phy. Chem. B 106 (2002) 9581.
[16] X.M. Ren, P. Zelenay, S. Thomas, J. Davey, S. Gottesfeld, J. Power Sources 86 (2000) 111.
[17] S. Wasmus, A. Kuver, J. Electroanal. Chem. 461 (1999) 14.
[18] K. Kordesch, G. Simader, Fuel Cells and Their Applications, VCH, Weinheim, Germany, 1996.
[19] S.J.C. Cleghron, X. Ren, T.E. Springer, M.S. Wilson, C. Zawodzinski, T.Z. Zawodzinski, S. Gottesfeld, Int. J. Hydrogen Energy 22 (1997) 1137.
[20] P.N. Ross Jr., in: J. Lipkowski, P.N. Ross Jr. (Eds.), Electrocatalysis, Frontiers of Electrochemistry, 4, Wiley/VCH, New York, 1998, p. 43.
[21] A. Hamnett, in: A. Wieckowski (Ed.), Interfacial Electrochemistry: Experimental Theory and Applications, 843, Marcel Dekker, New York, 1999.
[22] B.D. McNicol, D.A.J. Rand, K.R. Williams, J. Power Sources 83 (1999) 843.
[23] Gregor Hoogers, Fuel Cells Technology Hand Book, CRC press, Fl. USA, 2002.
[24] C.N. Tharamani, S.M. Mayanna, Electrochem. Solid State Lett. 9 (9) (2006) A412.
[25] C.N. Tharamani, F. Shafia Hoor, S.M. Noor Shahina Begum, Mayanna, J. Solid State Electrochem. 9 (2005) 476.
[26] T. Shobha, C.L. Aravinda, L. Gomathi Devi, S.M. Mayanna, J. Solid State Electrochem. 7 (2003) 451.
[27] L. Ramesh, B.S. Sheshadri, S.M. Mayanna, Int. Energy Res. 23 (10) (1999) 919.
[28] Weikang Hu, Yunshi Zhang, Deyiung Song, Zuoxiang Zhou, Wang. Yun, Mater. Chem. Phys. 41 (1995) 141.
[29] E. Jartych, M. Korolus, D. Oleszak, J.K. Zurawicz, J. Sarzynskiu, M. Budzyriski, J. Alloys Compd. 337 (2002) 69.
[30] Y. Choquette, H. Menard, L. Brossard, Int. J. Hydrogen Energy 14 (1989) 637.
[31] F.C. Crnkovic, S.A.S. Machado, L.A. Avaca, Int. J. Hydrogen Energy 29 (2004) 249.
[32] M. Bojinov, I. Betova, R. Raochoff, Electrochim. Acta 44 (1998) 721.
[33] D. Thierry, D. Persson, N. Leygraf, A. Boucherit, Hugot-le Goff, Corros. Sci. 32 (3) (1991) 27.
[34] S.M. Mayanna, T.H.V. Setty, Indian J. Chem. 10 (1972) 295.
[35] D. Briggs, M.P. Seah, Practical Surface Analysis by Auger and X-ray Photoelectron Spectroscopy, Wiley, New York, 1984, p. 503.
[36] T. Mimani, S.M. Mayanna, J. Appl. Electrochem. 23 (1993) 339.
[37] J. Grundy, G.A. Jones, The Structure, Properties of Solids 7: Electron Microscopy in the Study of Material, Crane Russak, New York, 1976, p. 19.
[38] A.M. Visco, F. Neri, G. Neri, A. Donato, C. Milone, S. Galvagno, Phys. Chem. Chem. Phys. 1 (1999) 2869.
[39] R.W. Guerfi, L.J. Paynter, Dao, J. Electrochem. Soc. 142 (1995) 3457.
[40] W Ying, R.F Estevao, C Gabriel, Z Yimin, I.A. Yasuyuki, C.R. Jose, C Carlos, J. Electrochem. Soc. 148 (2001) C222.
[41] J.H. Scofield, J. Electron Spectrosc. Relat. Phenom. 8 (1976) 129.
[42] D.R. Penn, J. Electron Spectrosc. Relat. Phenom. 9 (1976) 29.